SCIENTIFIC REPORTS

OPEN

SUBJECT AREAS:
COMPUTATIONAL SCIENCE
TWO-DIMENSIONAL MATERIALS
ELECTRONIC PROPERTIES AND DEVICES
ELECTRONIC AND SPINTRONIC DEVICES

Received
18 March 2013

Accepted
10 July 2013

Published
26 July 2013

Correspondence and requests for materials should be addressed to Z.W. (zhiwu@mines.edu)

Bandgap Opening by Patterning Graphene

Marc Dvorak, William Oswald & Zhigang Wu

Department of Physics, Colorado School of Mines, Golden, CO 80401, USA.

Owing to its remarkable electronic and transport properties, graphene has great potential of replacing silicon for next-generation electronics and optoelectronics; but its zero bandgap associated with Dirac fermions prevents such applications. Among numerous attempts to create semiconducting graphene, periodic patterning using defects, passivation, doping, nanoscale perforation, etc., is particularly promising and has been realized experimentally. However, despite extensive theoretical investigations, the precise role of periodic modulations on electronic structures of graphene remains elusive. Here we employ both the tight-binding modeling and first-principles electronic structure calculations to show that the appearance of bandgap in patterned graphene has a geometric symmetry origin. Thus the analytic rule of gap-opening by patterning graphene is derived, which indicates that if a modified graphene is a semiconductor, its two corresponding carbon nanotubes, whose chiral vectors equal graphene's supercell lattice vectors, are both semimetals.

Graphene has risen as a fascinating system in condensed matter physics for not only fundamental science but also technological applications[1–4] because of its many unique and amazing properties originating from its massless fermions[2,5] due to the linear dispersion of energy bands near the Dirac points (**K**). For example, under gate voltage charge carriers in graphene can be tuned continuously between electrons and holes[1], and their mobilities exceed 2.5×10^5 $cm^2V^{-1}s^{-1}$ under ambient conditions[6]. This certainly makes graphene extremely attractive for electronic and optoelectronic applications[3,4]; however, graphene is a semimetal with bandgap (E_g) closing at **K**, which prohibits switching off the graphene channels in field-effect transistors and building functional junctions in graphene optoelectronics.

Extraordinary efforts[7–16] have been spent to create semiconducting graphene materials that maintain the exceptional transport property. One scheme is obtaining bandgap through quantum confinement in graphene nanoribbons[7] (GNRs). But it is difficult to control the magnitude of bandgap in GNRs, since E_g is very sensitive to ribbon edge and width; moreover, a narrow GNR, which is necessary for a sizable gap, cannot carry sufficiently large currents. Other methods include substrate-induced[8,9] and strain-induced[10] bandgaps, but the former is essentially not tunable, while the latter is practically limited by the ability of tuning E_g to the desired value. An alternative approach is to periodically modify graphene[17], which is crucial to preserve its anomalously high charge carriers mobilities, by normal or inverse Stone-Thrower-Wales type of defects[11,12], hydrogen passivation[13], boron and nitrogen doping[14], and nanoscale holes creating graphene nanomeshes[15–17] (GNMs), etc. In particular, Balog *et al.*[13] demonstrated the existence of bandgap in graphene by patterned hydrogen adsorption, and Bai *et al.*[16] made functional GNM field-effect transistors capable of supporting currents 100 times of those in GNR-based devices.

However, it is still a mystery that a periodically modulated graphene can either open up a substantial gap or remain gapless (or a tiny gap) if its supercell lattice changes only slightly[18–28], which complicates the creation of bandgap by patterning and is apparently at odds with the proposal that bandgap in these graphene structures is due to quantum confinement between neighboring modulated sites[16]. The quantitative description of quantum confinement that results in energy gap in a patterned graphene is missing; instead, previous theoretical investigations[18–28] mainly focused on some special patterns whose supercell lattices form rectangular or hexagonal structures. A number of interesting empirical rules have been unraveled, but a fundamental and precise understanding on how electronic structures are affected by regularly patterning graphene has not yet been revealed.

Results

Analytical theory. In this work we adopt and extend the tight-binding model[2], which describes the sp^2-bonding in graphene extremely well, to include periodic structural alterations modeled by an external potential $U(\mathbf{r})$ applied

on graphene[29]. We denote the primitive lattice vectors of the pristine graphene by $\mathbf{a}_1$ and $\mathbf{a}_2$, and the supercell lattice vectors of the patterned graphene can be written as

$$\begin{aligned}\mathbf{R}_1 &= n_1\mathbf{a}_1 + m_1\mathbf{a}_2 \\ \mathbf{R}_2 &= n_2\mathbf{a}_1 + m_2\mathbf{a}_2\end{aligned} \tag{1}$$

with (n_1, m_1, n_2, m_2) four integers. If the perturbed sites form two-dimensional Bravais lattices, then the external potential $U(\mathbf{r})$ has the same translational symmetry

$$U(\mathbf{r}) = U(\mathbf{r} + l_1\mathbf{R}_1 + l_2\mathbf{R}_2), \tag{2}$$

where l_1 and l_2 are two integers.

At Dirac points $\mathbf{K}$, the intrinsic tight-binding off-diagonal matrix elements $\lambda_0 f(\mathbf{k})$ of the pristine graphene vanishes, giving rise to a zero bandgap; therefore, a non-vanishing $U(\mathbf{K})$, the Fourier transformation of $U(\mathbf{r})$ at Dirac points will result in an energy gap. This leads to the following bandgap opening rule:

$$\begin{cases} n_1 - m_1 = 3p \ \text{ and } \ n_2 - m_2 = 3q, & \text{(Gap opening)} \\ \text{Otherwise,} & \text{(Gap closure)} \end{cases} \tag{3}$$

where p and q are two integers. Our modeling is briefly summarized in the Methods section, and the physical reasoning and mathematical derivations are detailed in Supplementary Information.

Equation (3) indicates that only one ninth of arbitrarily patterned graphenes are semiconducting while the rest remain semi-metallic; thus the patterning periodicity must be carefully chosen to create a gap. Furthermore, Equation (1) suggests that a patterned graphene can be mapped to a pair of carbon nanotubes[30] (CNTs) with chiral vectors $\mathbf{C}_h$ equal to $\mathbf{R}_1$ and $\mathbf{R}_2$, respectively; then bandgap opening in a patterned graphene has an exactly opposite correlation to that in CNTs: it possesses a sizable bandgap only if *both of its corresponding CNTs are gapless* at the tight-binding level.

We illustrate our analytical theory by discussing a crucial and representative class of patterned graphene, namely GNMs. Fig. 1 plots various unit cells of GNMs, which are parallelograms with different angles, side lengths, and orientations with respect to the pristine graphene lattice. Because of the honeycomb structure of graphene, 60° and 90° (rectangle) parallelograms are especially important and have also been realized experimentally[15,16]. Like other patterned graphenes, a GNM can be mapped to two CNTs. Since unfolding a CNT generates a GNR, a GNM can also be mapped to a pair of GNRs, as illustrated in Figs. 1g and 1h. Experimentally, GNRs have been created by unzipping CNTs longitudinally[31], whereas CNTs could also be produced by wrapping GNRs around[32]. A GNR and its corresponding CNT have similar dependency of electronic band structure on their transverse vectors, and the well-known three-fold alternation in electronic structures is not surprising, given the hexagonal symmetry of graphene[2].

However, a GNM (or other types of patterned graphene)'s dependence of bandgap opening on supercell lattice vectors is oppositely to that of its corresponding CNTs (or GNRs), because along each lattice vector of a GNM the matching condition on Dirac points is exactly the same as the circular confinement condition of a CNT. A CNT is characterized by its chiral vector defined by a pair of integers (n, m): $\mathbf{C}_h = n\mathbf{a}_1 + m\mathbf{a}_2$. The tight-binding model asserts that a CNT is semi-metallic if $n - m \equiv 0 \bmod 3$, or semiconducting otherwise[30],

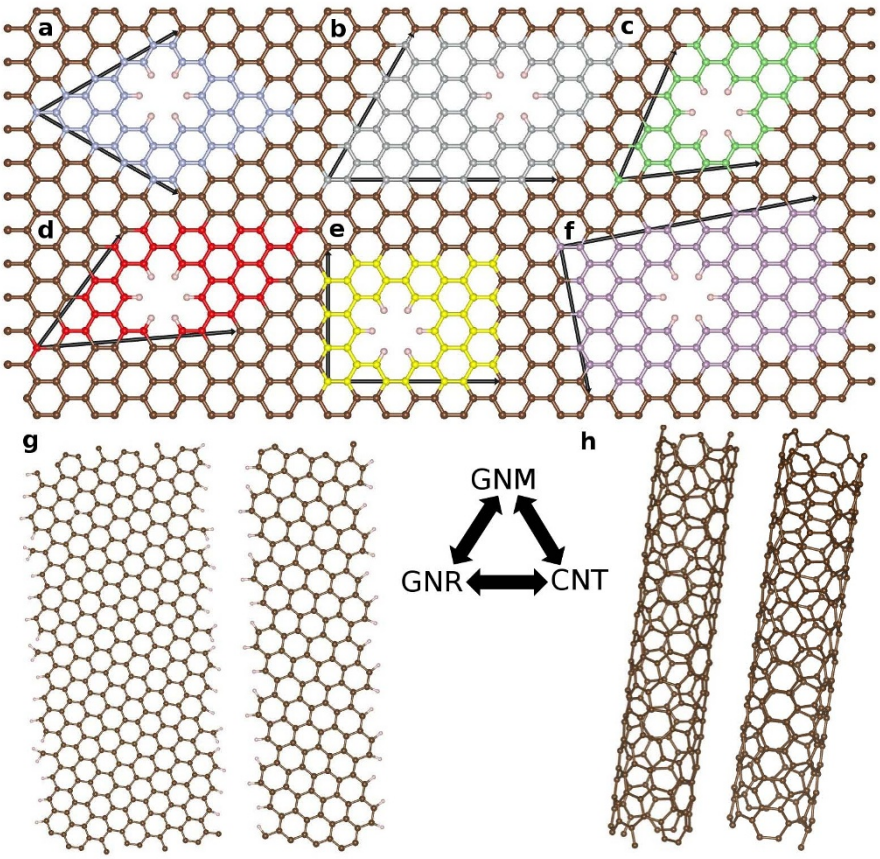

Figure 1 | Unit cells of GNMs. (a), (b) and (c) 60° parallelograms, with two lattice vectors along the zigzag (blue), armchair (gray) and chiral (green) directions, respectively. (d) Oblique parallelogram (red). (e) and (f) Rectangles whose lattice vectors are along the zigzag and armchair directions, respectively (yellow), or along two chiral directions (purple). Dangling bonds in GNMs and GNRs are passivated by hydrogen atoms (small gray dots), while carbon atoms are denoted by brown dots. (g) and (h) The relationship among GNMs, GNRs and CNTs, as explained in the text.

since its allowed **k** points satisfy $\mathbf{k} \cdot \mathbf{C}_h = 2\pi l$ with l integers. Figs. 2d–f illustrate that only when these lines of **k** points pass through graphene's Dirac points **K**, a CNT remains semimetallic. On the other hand, as shown in Figs. 2g–i, the reciprocal lattice vectors of a GNM are the intersections of two sets of parallel lines representing the allowed **k** points of its two matching CNTs. To create a bandgap, the reciprocal lattice vectors of a GNM must overlap the Dirac points, requiring both sets of parallel lines pass through **K**; consequently, a semiconducting GNM corresponds to two semimetallic CNTs.

First-principles calculations. In the following we demonstrate that the above conclusion drawn from analytical modeling is in excellent agreement with first-principles results. We present electronic structures obtained using the density functional theory (DFT[33,34]) for GNMs; in addition, our DFT calculations on periodically H-passivated and boron-nitrogen doped graphene show similar results, which will be published elsewhere. Although it is well known that DFT can severely underestimate bandgaps in semiconductors and insulators, DFT makes good predictions on the trends of electronic band structures and bandgap[35]. In particular, DFT correctly predicts a zero bandgap (closing at the Dirac points) for pristine graphene[2], and the predicted trends for bandgaps and band structures in graphene-based nanostructures, such as CNTs and GNRs, are mostly correct, compared with the many-body perturbation theory within the *GW* approximation and experimental data[7,30,36]. If these materials are semimetallic (or nearly semimetallic), DFT predicts them to have a zero (or nearly zero) bandgap; on the other hand, if they are semiconductors, DFT predicts sizable E_g, which tend to be underestimated.

Figs. 2j–l compare DFT electronic band structures of three oblique GNMs with $(n_1, m_1, n_2, m_2) = (9, -3, -4, 9), (7, 4, -4, 8)$ and $(9, -2, -4, 9)$, whose crystal structures are shown in Figs. 2g–i, respectively. Although these three GNMs have same holes and similar unit cells, only the middle one has a substantial gap because its two matching CNTs are semimetallic. The left GNM corresponding to one metallic and one semiconducting CNT, has a tiny gap at M_2 and it is nearly semimetallic; the GNM on the right remains gapless, with both of its matching CNTs semiconducting. These first-principles results agree well with our analytic theory, clearly demonstrating the sensitivity of

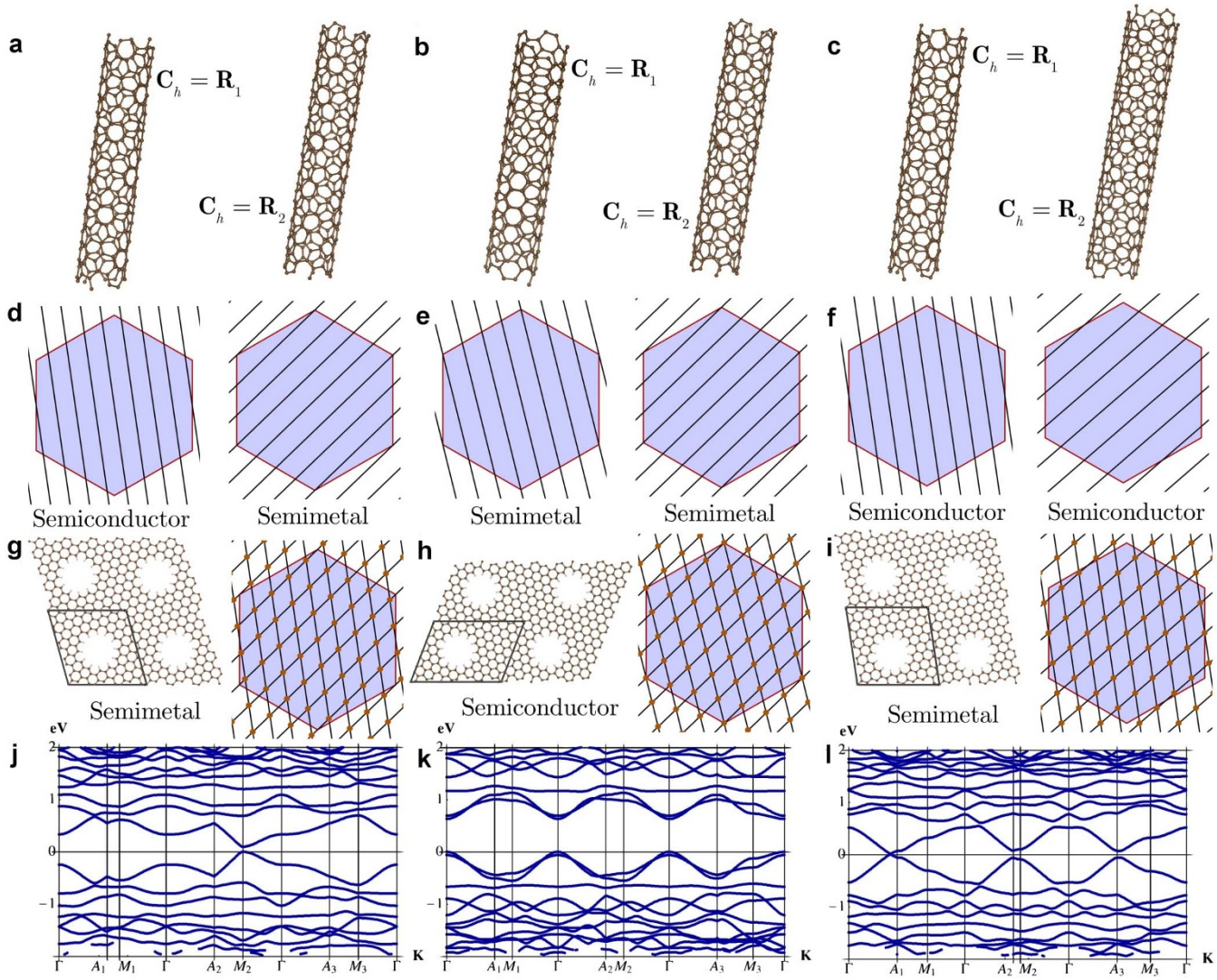

Figure 2 | Band gap opening/closure in GNMs and their corresponding CNTs. (a), (b) and (c) Crystal structures of a pair of CNTs in each panel, whose chiral vectors are equal to the lattice vectors of GNMs plotted on the left side of (g), (h) and (i), and whose allowed **k**-points (parallel lines) are plotted in (d), (e) and (f), respectively. The right side of (g), (h) and (i) show the reciprocal lattices of GNMs plotted in (a), (b) and (c), respectively. In (d)–(i) the hexagons indicate the Brillouin zone of the pristine graphene, with 6 corners the Dirac points. (j), (k) and (l) Electronic band structures of GNMs plotted in (g), (h) and (i), respectively. Brillouin zones of all GNMs in the text are plotted in Supplementary Fig. 2.

band structure to patterning periodicity, whose small variation could modify electronic structures significantly. They also suggest that in a GNM the top valence bands and bottom conduction bands derived from the π orbitals are nearly symmetric with respect to the Fermi energy (or the middle of energy gap), consistent with the tight-binding model for graphene in which only the nearest-neighbor interactions are taken into account.

Next we discuss rectangular and hexagonal GNMs, which have a one-to-one correlation to CNTs, because their lattice vectors $\mathbf{R}_1$ and $\mathbf{R}_2$ are not independent. $\mathbf{R}_1$ and $\mathbf{R}_2$ of a rectangular GNM form the chiral and translational (**T**) vectors of a CNT subject to an integer multiplier j: $\mathbf{R}_1 = \mathbf{C}_h$ and $\mathbf{R}_2 = j\mathbf{T}$, or $\mathbf{R}_1 = j\mathbf{T}$ and $\mathbf{R}_2 = \mathbf{C}_h$. Here $\mathbf{T} = t_1\mathbf{a}_1 + t_2\mathbf{a}_2$, with $t_1 = (2m + n)/t$, $t_2 = -(2n + m)/t$, and t the greatest common divisor of $2m + n$ and $2n + m$. If $n - m$ is not a multiple of 3, then $t_1 - t_2 \equiv 0 \bmod 3$; thus at least $n_1 - m_1$ or $n_2 - m_2$ is divisible by 3. We set $n_2 - m_2 \equiv 0 \bmod 3$, so that the existence of a bandgap in a rectangular GNM depends only on $\mathbf{R}_1$ by the difference between n_1 and m_1: it is semiconducting if $n_1 - m_1 \equiv 0 \bmod 3$ or semi-metallic otherwise, exactly in contrast to a CNT with $\mathbf{C}_h = \mathbf{R}_1$, as summarized in Fig. 3i. The DFT band structures of two rectangular GNMs (Figs. 3a and 3b) with $(n_1, m_1, n_2, m_2) = (6, 3, -4, 5)$ and $(6, 4, -7, 8)$ are plotted in Figs. 3e and 3f. In both cases $n_2 - m_2$ are divisible by 3; the former is a semiconductor with a direct gap at the Γ-point, while the latter is semimetallic with gap closing at the $\Gamma - M_2$ segment. In fact, all semiconducting GNMs open up a direct bandgaps at the Γ point.

In a rectangular GNM, $\mathbf{R}_1$ and $\mathbf{R}_2$ are perpendicular to each other with *conjugate* chiralities so that at least one of its two matching CNTs are metallic, and then one third of rectangular GNMs are semiconducting. On the other hand, a 60° parallelogram GNM's lattice vectors $\mathbf{R}_1$ and $\mathbf{R}_2$ have the same chirality subject to integer multipliers. In general we cannot assign a pair of integers to characterize a 60° parallelogram GNM, because $\mathbf{R}_1$ and $\mathbf{R}_2$ might be different in length. For $\mathbf{R}_1$ and $\mathbf{R}_2$ with the same length, a 60° parallelogram becomes a 60° rhombus and such GNMs have the hexagonal symmetry, in which $n_1 - m_1$ and $n_2 - m_2$ are either both divisible or neither divisible by 3. Therefore the existence of a bandgap in a hexagonal GNM also depends only on $\mathbf{R}_1$ by $n_1 - m_1$, and one third of them possess bandgaps, compared with only one ninth of 60° parallelogram GNMs semiconducting. Figs. 3g and 3h plot DFT band structures of two hexagonal GNMs (Figs. 3c and 3d) with $(n_1, m_1, n_2, m_2) = (5, 4, 9, -5)$ and $(7, 1, 8, -7)$, respectively. As predicted by Eq. (3), the former is semimetallic, while the latter is a semiconductor.

Previous theory and simulations[18–28] studied many special GNMs, namely the zigzag (Fig. 1a), armchair (Fig. 1b), and zigzag-armchair (Fig. 1e) GNMs, in which $\mathbf{R}_1$ and $\mathbf{R}_2$ are both along the zigzag or armchair direction, or along zigzag and armchair directions respectively. A zigzag GNM is characterized by a pair of integers (Z_1, Z_2) with $(n_1, m_1, n_2, m_2) = (Z_1, 0, 0, Z_2)$, an armchair by (A_1, A_2) with $(n_1, m_1, n_2, m_2) = (2A_1, -A_1, A_2, A_2)$ and a zigzag-armchair by (Z, A) with $(n_1, m_1, n_2, m_2) = (Z, -Z, A, A)$. The bandgap opening rules for these special cases as functions of structural parameters A and Z are presented in Figs. 4e, 4f and 4j, respectively. One third of zigzag-armchair GNMs are semiconducting, which is independent of the value of A and depends only on whether $Z \equiv 0 \bmod 3$. A zigzag GNM acquires a bandgap if both $Z_1 \equiv 0 \bmod 3$ and $Z_2 \equiv 0 \bmod 3$, so only one ninth of them are semiconducting, whereas *all* armchair GNMs

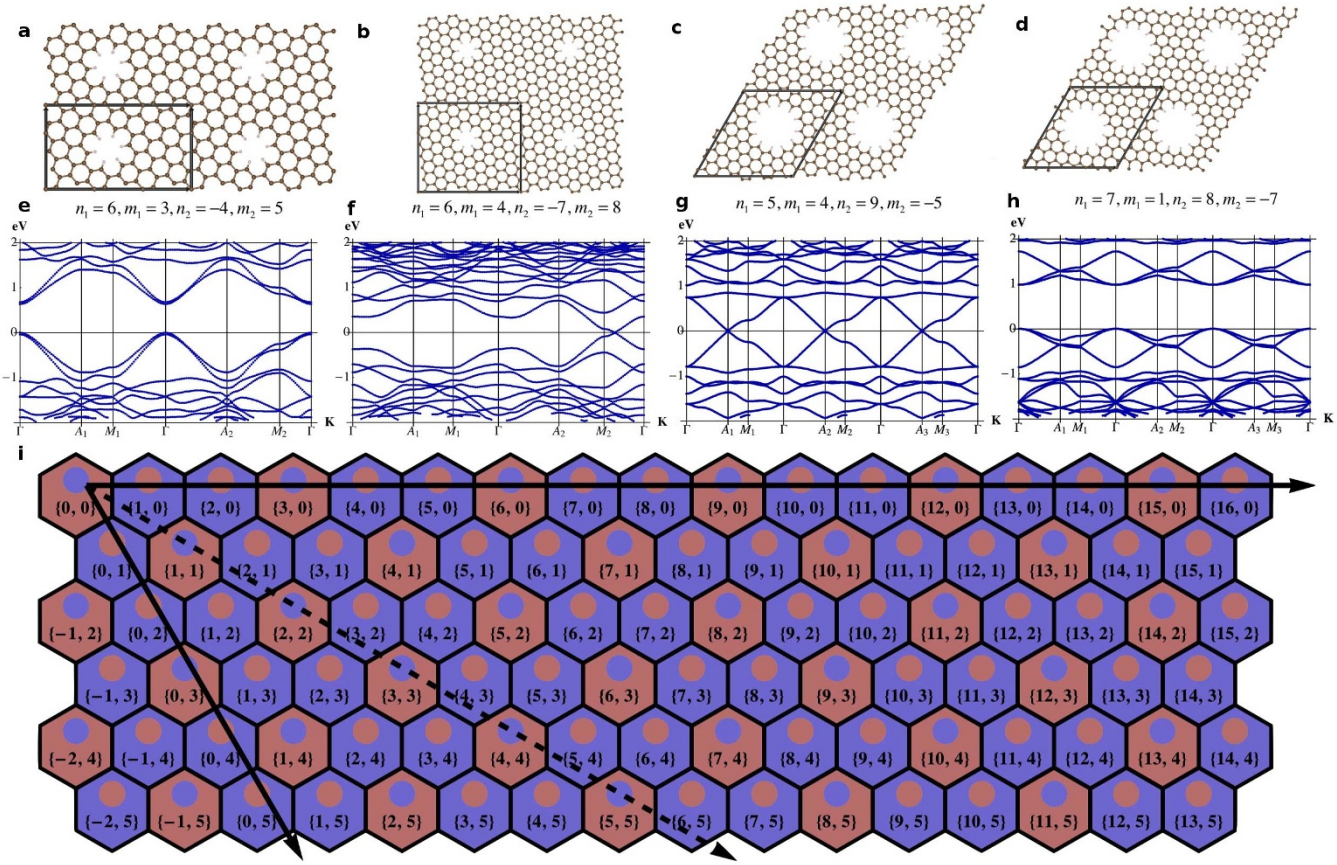

Figure 3 | Rectangular and hexagonal GNMs. (a) and (b) Crystal structures of two rectangular GNMs; (e) and (f) the corresponding electronic band structures. (c) and (d) Crystal structures of two hexagonal GNMs; (g) and (h) the corresponding electronic band structures. (i) Bandgap opening (red) and closure (blue) for rectangular and hexagonal GNMs (hexagons) and CNTs (circles) characterized by (n_1, m_1) for vector $\mathbf{R}_1$ of GNMs and $\mathbf{C}_h$ of CNTs, respectively, i.e., $\mathbf{C}_h = \mathbf{R}_1 = n_1\mathbf{a}_1 + m_1\mathbf{a}_2$. Here the solid arrows in (i) denote the zigzag direction, while the dashed line indicates the armchair vector.

are semiconductors regardless of the values of A_1 and A_2. These predictions have been verified by previous[18–28] and present DFT calculations whose results are plotted in Figs. 4a–d, 4g and 4h. Comparing band structures plotted in Figs. 2–4, one finds that for the same symmetry of patterning, semiconducting graphene alternates with semimetallic ones, except for the armchair case where all of them are semiconductors. Apparently, the armchair structure is the preferred choice to open bandgap by patterning graphene.

We have carried out additional DFT calculations for electronic structures of other patterned graphenes with a variety of unit cells and defect sizes other than what reported in Figs. 2–4. All these results (in Supplementary Information) agree with Equation (3) on bandgap existence. Furthermore, the magnitude of bandgap of a semiconducting patterned graphene depends on the onsite perturbation strength and inter-site distances; in particular, E_g of GNMs as functions of hole size and unit-cell area can be well fitted to a simple scaling rule proposed by Pedersen *et al.*[18], as demonstrated in Fig. 4i. Hence once a semiconducting patterning is chosen, E_g can be tuned to the ideal values for target applications by adjusting the types and sizes of and distances between structural modulations.

Discussion

Using a perturbative tight-binding model we have derived a universal bandgap opening rule for graphene with arbitrary Bravais periodic patterning. A simple reverse relation on existence of bandgap between a modified graphene and its two analogous CNTs is found, which is confirmed by first-principles electronic structure calculations. Current modeling can be easily generalized from Bravais to non-Bravais supercells, such as the honeycomb structure, and thus the DFT results for the honeycomb GNMs[26] can also be well explained. We conclude that bandgap opening in patterned graphene is not directly caused by quantum confinement as in CNTs or GNRs, though confinement still plays a role in determining the magnitude of E_g once a gap is present; instead, it originates from geometric symmetry breaking at the Dirac points, leading to the exactly opposite bandgap opening conditions between modified graphene and CNTs.

Thus our present work has solved an outstanding problem on how to properly pattern graphene to induce bandgaps, pointing to practical routes of geometrically designing graphene with controllable and desirable electronic behaviors. Previous experiments[13–17] have demonstrated that patterning graphene could open up a substantial bandgap suitable for transistors, but none of them have yet reported the predicted sensitivity of electronic behavior to patterning periodicity. Their patterned graphene structures are rather rough, which might greatly hamper transport of charge carriers, while a high-quality accurate periodic patterning is expected to largely maintain the ultrahigh electron mobility. This requires the ability of tailoring

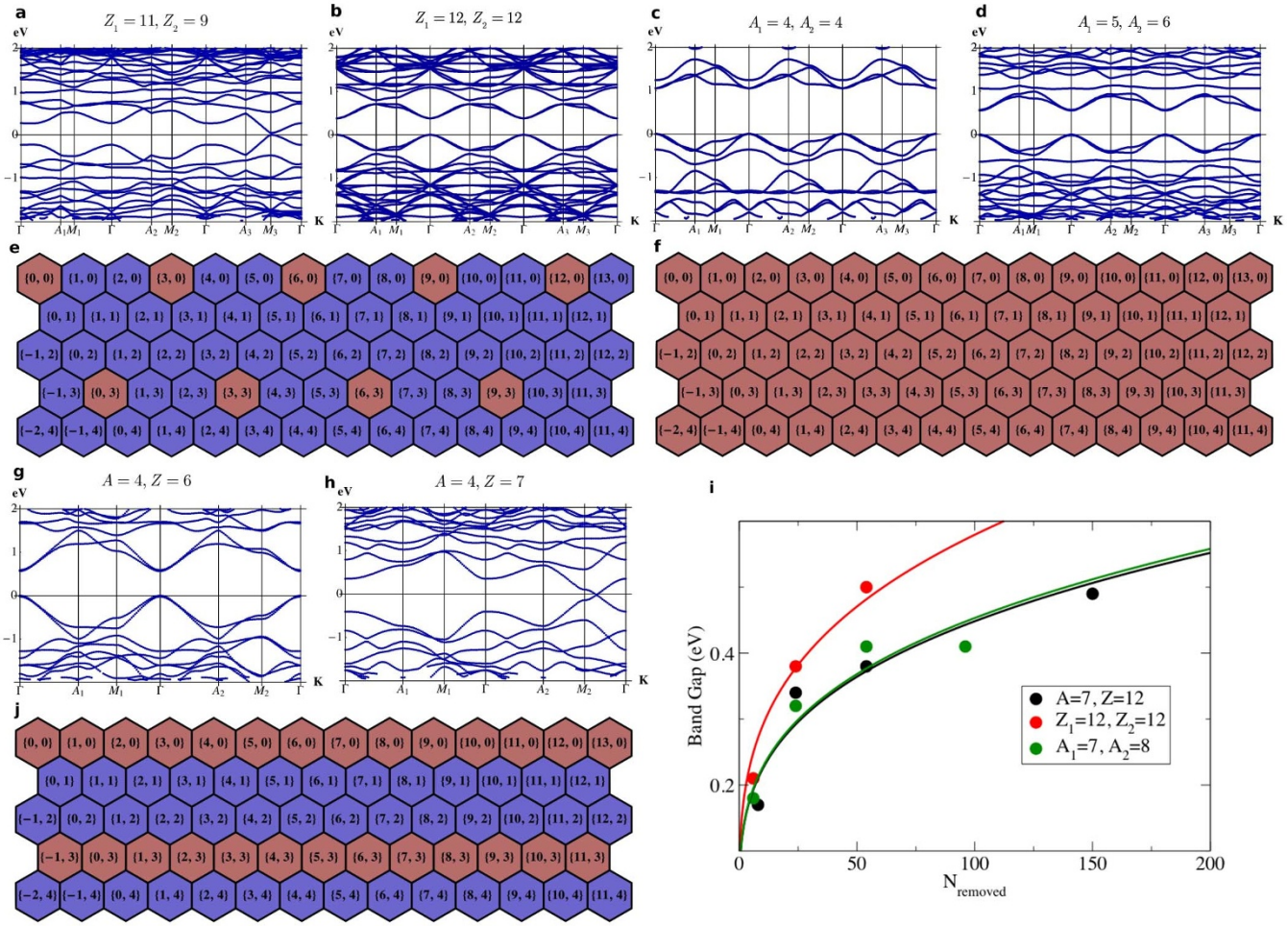

Figure 4 | Zigzag, armchair, and zigzag-armchair GNMs. Electronic band structures of two zigzag (a, b), armchair (c, d), and zigzag-armchair (g, h), GNMs. Their crystal structures are plotted in Supplementary Fig. 3. (e), (f) and (j). Band gap opening (red) and closure (blue) for zigzag (e), armchair (f) and zigzag-armchair (j) GNMs characterized by (Z_1, Z_2), (A_1, A_2) and (A, Z), respectively. (i) Bandgap (eV) as a function of hole size indicated by the number of removed carbon atoms ($N_{removed}$) per unit cell for a zigzag (red), an armchair (green) or a zigzag-armchair (black) GNM. Computed data (closed circles) are fitted to smooth curves, as described in Supplementary Information.

graphene structures precisely at the atomic scale[37] – an exciting and rapidly advancing frontier in nanoscience and nanotechnologies for realizing electronics and optoelectronics towards ever smaller length scales.

Finally, the restriction of our modeling, as well as the key to its success, is that the valence and conduction bands in graphene touch only at the Dirac points. In other materials with vanishingly small density of states near the Fermi energy or, equivalently, bandgap closing only at a small discrete set of **k** points, it is possible to perturb all these touching **k** points by patterning. Moreover, it is appealing to investigate the effects of periodic perturbation and structural symmetry breaking on strongly-correlated materials showing intriguing quantum/topological orders, such as topological insulators[38], whose gapless surface states are protected by time-reversal symmetry and the topology of the material.

Methods

First-principles calculations. Our first-principles electronic structure calculations based on DFT were performed employing the SIESTA package[39] using a triple-ζ polarized atomic basis set for carbon atoms, whose numerical accuracy has been rigorously examined against the planewave-based VASP program[40]. The two-dimensional Brillouin zones of GNMs were sampled on a 2×2 Monkhorst-Pack **k**-grid with good convergence due to very large unit cells. The generalized gradient approximation[41] was used for the exchange-correlation functional. All calculations are spin-polarized. GNM structures are optimized until the maximum atomic force is less than 0.02 eV/Å. Dangling bonds in GNMs are passivated by hydrogen atoms.

Tight-binding model. Graphene has two sublattices (A and B) whose Hamiltonian is written as

$$H_{\mathbf{K}} = \begin{pmatrix} E_0 & \lambda_0 f(\mathbf{k}) \\ \lambda_0 f^*(\mathbf{k}) & E_0 \end{pmatrix}, \tag{4}$$

where E_0 and λ_0 are two parameters. The eigenvalues are

$$E_{\pm}(\mathbf{k}) = E_0 \pm \lambda_0 |f(\mathbf{k})|, \tag{5}$$

$$|f(\mathbf{k})| = \sqrt{3 + 2\cos\left(\sqrt{3}k_y a\right) + 4\cos\left(\frac{\sqrt{3}}{2}k_y a\right)\cos\left(\frac{3}{2}k_x a\right)}, \tag{6}$$

with $a \approx 1.42$ Å, the neighboring carbon-carbon distance. The structural modifications are modeled by an external periodic potential $U(\mathbf{r})$. If the scattering matrix element between two degenerate pseudo-spin states at the Dirac points

$$\lambda_1(\mathbf{K}) = N\langle\phi_A|U(\mathbf{K})|\phi_B\rangle, \tag{7}$$

is non-zero, where ϕ_A and ϕ_B are orbitals for a pair of the nearest neighbors, N is the effective average number of the nearest neighbors per site, and $U(\mathbf{k})$ is the Fourier transformation of $U(\mathbf{r})$, or the scattering matrix element between two degenerate states at Dirac points $\mathbf{K}$ and $\mathbf{K}'$[42,43]

$$|\langle\mathbf{K}|U_r|\mathbf{K}'\rangle|^2 = |U(\mathbf{K}'-\mathbf{K})|^2\cos^2(\theta_{\mathbf{K},\mathbf{K}'}/2), \tag{8}$$

is non-zero, where $\theta_{\mathbf{K},\mathbf{K}'}$ is the angle between $\mathbf{K}$ and $\mathbf{K}'$, then there is a sizable bandgap in the defected graphene. Eqs. 7 and 8 lead to the same bandgap opening condition of $U(\mathbf{K}) \neq 0$.

1. Geim, A. K. & Novoselov, K. S. The rise of graphene. *Nature Mater.* **6**, 183–191 (2007).
2. Castro Neto, A. H., Guinea, F., Peres, N. M. R., Novoselov, K. S. & Geim, A. K. The electronic properties of graphene. *Rev. Mod. Phys.* **81**, 109–162 (2009).
3. Schwierz, F. Graphene transistors. *Nature Nanotech.* **5**, 487–496 (2010).
4. Novoselov, K. S. *et al.* Roadmap for graphene. *Nature* **490**, 192–200 (2012).
5. Novoselov, K. S. *et al.* Two-dimensional gas of massless Dirac fermions in graphene. *Nature* **438**, 197–200 (2005).
6. Mayorov, A. S. *et al.* Micrometer-scale ballistic transport in encapsulated graphene at room temperature. *Nano Lett.* **11**, 2396–2399 (2011).
7. Son, Y. W., Cohen, M. L. & Louie, S. G. Energy gaps in graphene nanoribbons. *Phys. Rev. Lett.* **97**, 216803 (2006).
8. Zhou, S. Y. *et al.* Substrate-induced bandgap opening in epitaxial graphene. *Nature Mater.* **6**, 770–775 (2007).
9. Hicks, J. *et al.* A wide-bandgap metal–semiconductor–metal nanostructure made entirely from graphene. *Nature Phys.* (2012).
10. Choi, S.-M., Jhi, S.-H. & Son, Y.-W. Effects of strain on electronic properties of graphene. *Phys. Rev. B* **81**, 081407 (2010).
11. Lusk, M. T. & Carr, L. D. Nanoengineering defect structures on graphene. *Phys. Rev. Lett.* **100**, 175503 (2008).
12. Lahiri, J., Lin, Y., Bozkurt, P., Oleynik, I. I. & Batzill, M. An extended defect in graphene as a metallic wire. *Nature Nanotech.* **5**, 326–329 (2011).
13. Balog, R. *et al.* Bandgap opening in graphene induced by patterned hydrogen adsorption. *Nature Mater.* **9**, 315–319 (2010).
14. Ci, L. *et al.* Atomic layers of hybridized boron nitride and graphene domains. *Nature Mater.* **9**, 430–435 (2010).
15. Eroms, J. & Weiss, D. Weak localizations and transport gap in graphene antidote lattices. *New J. Phys.* **11**, 095021 (2009).
16. Bai, J., Zhong, X., Jiang, S., Huang, Y. & Duan, X. Graphene nanomesh. *Nature Nanotech.* **5**, 190–194 (2010).
17. Kim, M., Safron, N. S., Han, E., Arnold, M. S. & Gopalan, P. Fabrication and characterization of large-area, semiconducting nanoperforated graphene materials. *Nano Lett.* **10**, 1125 (2010).
18. Pedersen, T. G. *et al.* Graphene antidot lattices: designed defects and spin qubits. *Phys. Rev. Lett.* **100**, 136804 (2008).
19. Allison, K. F., Borka, D., Radovic Hadzievski, L. J. & Miskovic, Z. L. Dynamic polarization of graphene by moving external charges: Random phase approximation. *Phys. Rev. B* **80**, 195405 (2009).
20. Liu, W., Wang, Z. F., Shi, Q. W., Yang, J. & Liu, F. Band-gap scaling of graphene nanohole superlattices. *Phys. Rev. B* **80**, 233405 (2009).
21. Fürst, J. A. *et al.* Electronic properties of graphene antidot. *New J. Phys.* **11**, 095020 (2009).
22. Baskin, A. & Prál, P. Electronic structures of porous nanocarbons. *Sci. Rep.* **1**, 36 (2011).
23. Sahin, H. & Ciraci, S. Structural, mechanical, and electronic properties of defect-patterned graphene nanomeshes from first principles. *Phys Rev. B* **84**, 035452 (2011).
24. Cui, X. Y. *et al.* Magic numbers of nanoholes in graphene: tunable magnetism and semiconductivity. *Phys. Rev. B* **84**, 125410 (2011).
25. Petersen, R., Pedersen, T. G. & Jauho, A. P. Clar sextet analysis of triangular, rectangular, and honeycomb graphene antidot lattices. *ACS Nano* **5**, 523–529 (2011).
26. Ouyang, F. P., Peng, S., Liu, Z. & Liu, Z. Bandgap opening in graphene antidot lattices: the missing half. *ACS Nano* **5**, 4023–4030 (2011).
27. Oswald, W. & Wu, Z. Energy gaps in graphene nanomeshes. *Phys. Rev. B* **85**, 115431 (2012).
28. Feng, J. *et al.* Patterning graphene. *Nanoscale* **4**, 4883 (2012).
29. Park, C.-H., Yang, L., Son, Y.-W., Cohen, M. L. & Louie, S. G. Anisotropic behaviours of massless Dirac fermions in graphene under periodic potentials. *Nature Phys.* **4**, 213–217 (2008).
30. Charlier, J. C., Blase, X. & Roche, S. Electronic and transport properties of nanotubes. *Rev. Mod. Phys.* **79**, 677–732 (2007).
31. Kosynkin, D. V. *et al.* Longitudinal unzipping of carbon nanotubes to form graphene nanoribbons. *Nature* **458**, 872–876 (2009).
32. Kit, O. O., Tallinen, L., Mahadevan, L., Timonen, J. & Koskinen, P. Twisting graphene nanoribbons into carbon nanotubes. *Phys. Rev. B* **85**, 085428 (2012).
33. Hohenberg, P. & Kohn, W. Inhomogeneous electron gas. *Phys. Rev.* **136**, B864 (1964).
34. Kohn, W. & Sham, L. J. Self-consistent equations including exchange and correlation effects. *Phys. Rev.* **140**, A1133 (1965).
35. Onida, G., Reining, L. & Rubio, A. Electronic excitations: density-functional versus many-body Green's-function approaches. *Rev. Mod. Phys.* **74**, 601 (2002).
36. Yang, L., Park, C.-H., Son, Y.-W., Cohen, M. L. & Louie, S. G. Quasiparticle energies and band gaps in graphene nanoribbons. *Phys. Rev. Lett.* **99**, 186801 (2007).
37. Tapasztó, L., Dobrik, G., Lambin, P. & Biró, L. P. Tailoring the atomic structure of graphene nanoribbons by scanning tunnelling microscope lithography. *Nature Nanotech.* **3**, 397 (2008).
38. Qi, X.-L. & Zhang, S.-C. Topological insulators and superconductors. *Rev. Mod. Phys.* **83**, 1057–1110 (2011).
39. Soler, J. M. *et al.* The SIESTA method for ab-initio order-*N* materials simulation. *J. Phys: Cond. Matt.* **14**, 2745 (2002).
40. Kresse, G. & Furthmüller, J. Efficient iterative schemes for ab-initio total-energy calculations using a plane-wave basis set. *Phys. Rev. B* **54**, 11169–11186 (1996).
41. Perdew, J. P., Burke, K. & Ernzerhof, M. Generalized gradient approximation made simple. *Phys. Rev. Lett.* **77**, 3865 (1996).
42. Ando, T. & Nakanishi, T. Impurity scattering in carbon nanotubes – absence of back scattering. *J. Phys. Soc. Japan* **67**, 1704–1713 (1998).
43. Ando, T., Nakanishi, T. & Saito, R. Berry's phase and absence of back scattering in carbon nanotubes. *J. Phys. Soc. Japan* **67**, 2857–2862 (1998).

Acknowledgements

Z.W. gratefully acknowledges financial support from USA Department of Energy (DOE) Early Career Award (No. DE-SC0006433). Computations were carried out at the Golden Energy Computing Organization (GECO) at Colorado School of Mines and at National Energy Research Scientific Computing Center (NERSC).

Author contributions

Z.W. conceived and designed this project and derived the theoretical modeling. M.D. was involved in analytical derivations and performed first-principles calculations. W.O. carried out some initial calculations. Z.W. and M.D. wrote the paper.

Additional information

Supplementary information accompanies this paper at http://www.nature.com/scientificreports

Competing financial interests: The authors declare no competing financial interests.

How to cite this article: Dvorak, M., Oswald, W. & Wu, Z. Bandgap Opening by Patterning Graphene. *Sci. Rep.* **3**, 2289; DOI:10.1038/srep02289 (2013).